Lab on a Chip

Cite this: *Lab Chip*, 2012, **12**, 3016–3019

www.rsc.org/loc

COMMUNICATION

Microfluidic cell volume sensor with tunable sensitivity†

Jason Riordon, Maryam Mirzaei and Michel Godin*

Received 13th April 2012, Accepted 6th June 2012
DOI: 10.1039/c2lc40357a

We report the fabrication and validation of a microfluidic cell volume sensor integrated on a multi-layered polydimethylsiloxane (PDMS) microchip with a tunable detection volume for dynamic control of sensitivity, enabling the detection of individual *Escherichia coli* and microparticles.

The development of microfluidic cell volume sensors has been fuelled by a need for biological detection capabilities in a low-cost, portable and energy-efficient format. Impedance-based volume sensors[1] and micro-Coulter counters[2,3] monitor the variation in ionic current through a narrow sensing region as individual micro-sized particles transit through. Prototypes have been developed to measure the size of a number of biological targets including individual red blood cells,[1] yeast[4] and *Escherichia coli*.[5] Maximum sensitivity is attained by fabricating a sensing channel similar to the dimensions of the target particle. Unfortunately, this both limits the device to targets of a narrow size range, and increases the chance of clogging.

In an effort to increase the dynamic range, some have used hydrodynamic focusing[5–8] to accommodate a broader range in target sizes. By flowing a conductive sheath of liquid between parallel nonconductive sheaths in a low-Reynolds number microfluidic environment, the electrolytic volume is reduced and sensitivity increased. Thus, effective sensing volume can be optimised without risk of obstruction. However, diffusion between sheaths could pose issues during experiments requiring much reduced or stopped flows, or in long-term trapping experiments requiring the introduction of various drugs.[4,9]

Another approach to increasing dynamic range while mitigating these issues is to integrate a tunable valve above the sensing channel. Multilayer soft lithography allows for the integration of valves and pumps into PDMS-based microfluidic devices.[10,11] Pressurizing a valve chamber above a microfluidic channel enables dynamic control of the channel height (Fig. 1a). By measuring electrical conductance in electrolytic media, channel volume is accurately characterized.[12] The sensing volume becomes tunable over a wide range (0.5 pL to 23 pL in the following examples), and can not only heighten sensitivity, but also allow the detection of smaller diameter microspheres (~1 μm) that would otherwise pass undetected. The moulded PDMS is bonded to a glass slide patterned with 80 nm thick Ag electrodes (deposited by electron beam physical vapor deposition with a 5 nm Cr adhesion layer). By pressurizing the valve, the PDMS membrane separating the fluidic and the pneumatic valve layers is adjusted to alter the volume of electrolytic solution separating the electrodes (Fig. 1c,d). The resistance (R) of the sensing volume is that of a conductor of uniform cross section (A) and length (l) (electrode separation): $R = \alpha\rho l/A$, where ρ is the resistivity the electrolyte and α is a geometrical factor due to the use of planar electrodes.[13] A micro-sized target in transit through the detection volume will cause a momentary increase in resistance as the electrolyte is displaced.

The device consists of two parallel 80 μm wide bypass microchannels connected by a narrow sensing channel, as depicted in Fig. 1b. Multiple designs were evaluated, with sensing channel widths ranging from 10 μm to 50 μm, and having 10 μm to 20 μm heights. Electrode width/separation varied between 15 μm and 25 μm. Two photoresists were tested as moulds for PDMS channels, SU-8 10 (MicroChem) and P4620 (AZ Electronic

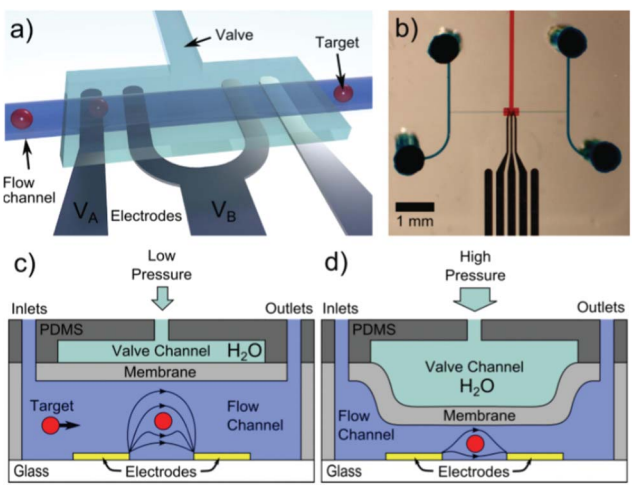

Fig. 1 a) Device schematic illustrating the valve, flow channel, electrodes, and targets. Only the two leftmost electrodes are utilised, labelled V_A and V_B. b) Volume sensor with flow channels (blue), valve (red) and electrodes (black). A central sensing channel links two wider channels, which serve as inlet and outlet. c) Cross-section of device illustrating the PDMS channel layer (light grey) and valve layer (dark grey). As targets flow between sensing electrodes, electrolytes are displaced resulting in a drop in conductance proportional to target volume. d) In pressurizing the valve, sensing volume is reduced and sensitivity increased.

Physics Department, University of Ottawa, Ottawa, Ontario, Canada K1N 6N5. E-mail: michel.godin@uottawa.ca
† Electronic Supplementary Information (ESI) available: Fabrication details and flow control. See DOI: 10.1039/c2lc40357a

Materials). SU-8 was used to create channels of 10 μm and 20 μm width, whereas P4620 was used to make 30 μm and 50 μm flow channels. The fabrication protocol for P4620 lead to channels with rounded features, meant to facilitate channel compression during valve pressurization.[10] Complete fabrication details are presented as ESI, section S1†.

The volume sensor operates by applying an AC potential between a pair of sensing electrodes and monitoring changes in current as transiting target microspheres disrupt ionic current. A function generator (Stanford Research Systems DS345) provides a 50 kHz, 30 mV signal to a low-noise preamplifier operating at unity gain (Stanford Research Systems SR560). The output voltage is applied to a first electrode V_A with respect to ground. The current collected by the other electrode is sent to a current amplifier (Keithley 428) which converts the ~5 μA signal to 0–10 V, which is monitored by a lock-in amplifier (Stanford Research Systems SR830 DSP). The lock-in signal is acquired at 200 kHz with a 16-bit DAQ card (NI USB-6353) and monitored *via* a LabView script. Each data set is subjected to a filtering algorithm using a combination of point-by-point averaging, Savitzky-Golay and lowpass filtering. Flow through the flow channel was controlled using pressure regulators (Bellofram Type 10). The pneumatic valve was also controlled by a pressure regulator (SMC IR2010-N02-R), and filled with deionized water to prevent air bubble formation in the flow channel during pressurization. A flow control diagram is presented in ESI section S2†.

The channel cross-section was calibrated during valve activation by fluorescence imaging;[10] intensity counts were converted to a channel height by combining them with profilometer measurements of the corresponding master mould. Fig. 2a and b show typical cross sections of two channels of different height and width. Channel cross-section is altered symmetrically as valve pressure is ramped up. The shape of the channel prior to valve activation determines how the collapse will progress: a square channel will show increased depression at the centre, where it is structurally weakest, whereas round channels display a more uniform compression. In the case of a square channel, high valve pressure (>15 psi) causes the sensing channel to split axially into two parallel channels. Fig.2c and d show optical microscope images of the sensing volume with an uncompressed and fully compressed valve, respectively. At a valve pressure of 28 psi, the channel is reduced to 2% of its original volume.

Polystyrene microspheres of different sizes were used to evaluate device performance over its entire range: d = 1.51 ± 0.05 μm, 3.9 ± 0.3 μm, 6.0 ± 0.4 μm and 7.3 ± 0.5 μm (Bangs Labs). Microsphere solutions were stripped of their buffer through multiple centrifugation/dilution steps, and then resuspended in an aqueous solution containing 0.1 M KCl, 1% bovine serum albumin (BSA) and 13% glycerol to a concentration between 10^5 and 10^7 particles mL^{-1}; BSA helps prevent microsphere agglomeration and glycerol ensures neutral buoyancy. A 0.1 M KCl solution was chosen to mimic conditions necessary to sustain living cells.

Fig. 3a illustrates a typical current change observed during the transit of d = 7.3 μm microspheres through the sensing region at different valve pressures for a 20 μm high by 50 μm wide channel (P4620 mould). Relative changes in current become stronger as channel is compressed. Fig.3b illustrates histograms obtained at four valve pressures for the d = 1.51 μm microspheres for a 20 μm high by 10 μm wide channel (SU-8 mould). Current drops corresponding to microbead pairs were removed for clarity.

These small microspheres were not detected until a 22.5 psi pressure was applied to the valve. Gaussian fits were taken for each data set, and show a clear widening effect associated with smaller detection volumes. Since the measurement is limited by sample polydispersity, Gaussian width will increase for smaller detection volumes.

Fig. 3c illustrates a compilation of current variations for various microspheres and valve configurations for the same device as for Fig.3a. The valve was pressurized to 0 , 4 and 8 psi. Linearity is demonstrated for each valve setting, with slopes of 2.31 ± 0.06, 3.40 ± 0.04 and 5.6 ± 0.2 (%/aL) for the d = 3.9 μm, d = 6.0 μm and d = 7.3 μm targets, respectively. The slope represents the sensitivity of the device operating at a given valve pressure, which reflects the geometry of the system as well as the preferred path taken by the target through the sensor. A sharper slope at increased valve pressure signifies a heightened sensitivity.

Moreover, in collapsing the channel, microspheres are forced to follow an alternate route through the sensing region. Finite element method (FEM) modeling with a FEMLAB toolkit (Comsol Ltd) shows a high dependence on vertical positioning: targets flowing near the electrodes alter electric field lines more significantly, thus further enhancing sensitivity. This impedance sensitivity height dependence has been previously reported.[14,15] Standard deviations obtained from current change histograms

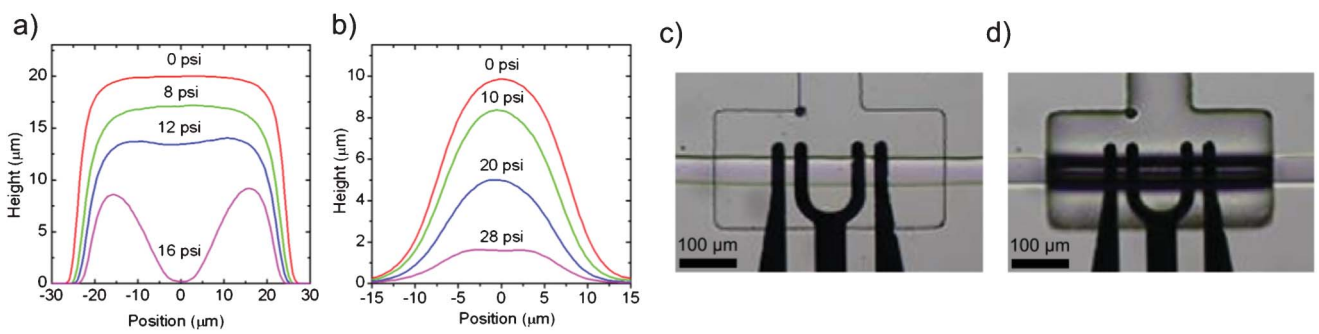

Fig. 2 Cross-section profile for different valve pressures obtained through fluorescence imaging and profilometer measurement of the P4620 mould for (a) 20 μm high by 50 μm wide channel and (b) 10 μm high by 30 μm wide channel. c) and d) are optical microscope images of an uncompressed and compressed valve, respectively, operating on the 20 μm high by 50 μm wide channel. Channel pressure is 3 psi; valve pressure switches from 0 to 28 psi.

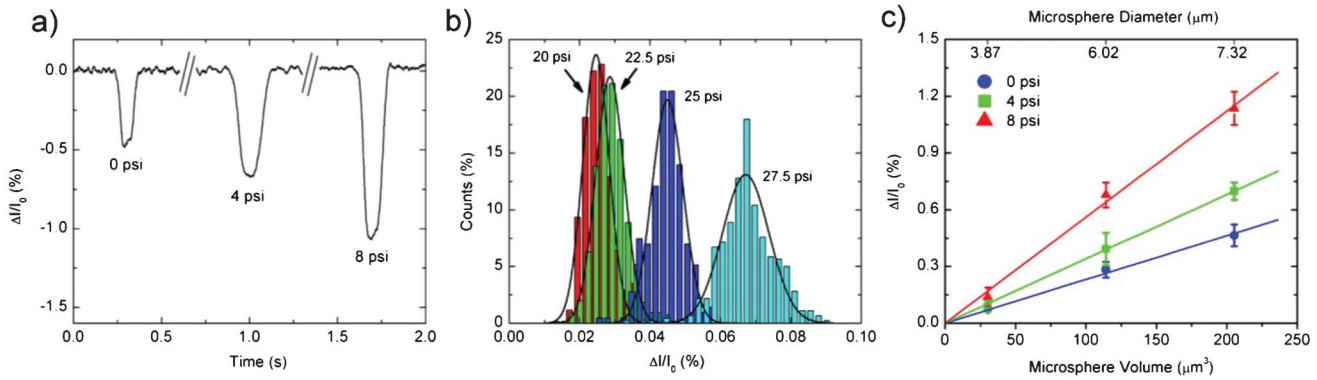

Fig. 3 a) Typical signal obtained by monitoring current as a $d = 7.3$ μm microsphere traverses the sensing region in a 20 μm high by 50 μm wide channel. Shown is the change in current ΔI relative to baseline current I_0. b) Histograms depicting relative change in current obtained from 2046 counts for $d = 1.51$ μm microspheres at variable valve height for a 20 μm high by 10 μm wide channel. c) Current change as a function of microsphere volume for $d = 3.9$, 6.0 and 7.3 μm microspheres on 20 μm high by 50 μm wide channel. A linear relation is observed at all configurations, showing increased sensitivity for a compressed channel. Flow channel pressure is kept constant at ~3 psi, with bypass channels at slightly offset pressures to induce a net flow through the sensor.

were converted to standard deviations on volume, and compared to that provided by the manufacturer. For most datasets, these matched quite well. However, for the $d = 7.3$ μm microbeads it was found to be about half of that indicated by the manufacturer through a commercial Coulter counter. A reduced standard deviation was also reported by Sridhar *et al.*[2] for $d = 9.8$ μm microsphere population (Bangs Labs), and remains puzzling. Table 1 lists the signal-to-noise ratio (SNR) measured for various microspheres under different valve configuration on this same device. While valve pressurization leads to improved SNR, the ratio of standard deviation to mean value in population measurements is not always improved. In effect, microspheres become easier to detect, but also show greater population variability. This could be improved by using an alternate electrode geometry, which would produce a more uniform electric field through the sensing volume.

To demonstrate the device's functionality for biological samples, a population of wild-type *E. coli* K12 was analyzed with a 20 μm high by 50 μm wide sensing channel (Fig. 4). Cells were suspended in LB broth at 10^8 cells mL^{-1}, and flowed through the sensor at a valve pressure of 20 psi (4 psi channel pressure). The valve pressure was chosen so as to be at the threshold where targets can pass, but only just. The size distribution is log-normal.[16]

In addition to heightened sensitivity, a volume sensor with a compressible sensing region provides the user with a means to easily dislodge a clog in the sensing volume. If there is a clog, a reduction in valve pressure quickly liberates the device. This flexibility allows the device to be used to study large particles that run the risk of damaging a static device. It is believed that cell

Table 1 Signal-to-noise ratio (SNR)

	Valve pressure (psi)				
Diameter (μm)	0	4	8	12	16
1.51	[a]	[a]	[a]	1.7	4.1
3.9	10	11	16	40	[b]
6.0	56	85	130	[b]	[b]
7.3	69	110	190	[b]	[b]

[a] SNR at sub-detection threshold. [b] Microspheres obstructed.

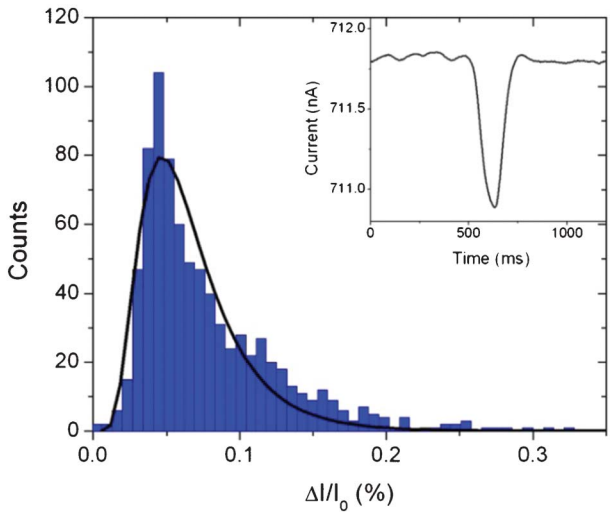

Fig. 4 Histogram depicting relative change in current for a population of K12 wild-type *E. coli*, fitted to a log-normal function. Calibration with $d = 1.51$ μm microspheres indicates an *E. coli* cell volume of 1.3 ± 0.3 μm^3. Inset graph shows current variation during a typical detection event.

volume sensor sensitivity could be further increased by improved electrical shielding through use of a Faraday cage. Long-term signal drift, while not crucial to transient current shift measurements, could be limited through the use of a temperature controller, since electrolytic conductivity is temperature dependent.

Conclusions

The microfluidic cell volume sensor enhanced with a pneumatic valve provides heightened sensitivity and dynamic range, allowing for the detection of live *E. coli* and smaller diameter microspheres (~1 μm) that would otherwise go undetected. Future work will focus on trapping cells for growth measurement, and automating valve compression to dynamically adjust channel height based on target volume.

Acknowledgements

The authors thank Ian Jardine, Jeff Salvail, Dominique Laniel and Eric Hoogkamp for preliminary modelling and microfabrication. This work is supported by the Natural Sciences and Engineering Research Council of Canada (NSERC) and the Canadian Foundation for Innovation (CFI).

References

1 K. Cheung, S. Gawad and P. Renaud, *Cytometry, Part A*, 2005, **65**, 124–132.
2 M. Sridhar, D. Xu, Y. Kang, A. B. Hmelo, L. C. Feldman, D. Li and D. Li, *J. Appl. Phys.*, 2008, **103**, 104701.
3 W. H. Coulter, *Proc. Natl. Electron. Conf.*, 1956, **12**, 1034.
4 J. Sun, C. C. Stowers, E. M. Boczko and D. Li, *Lab Chip*, 2010, **10**, 2986.
5 C. Bernabini, D. Holmes and H. Morgan, *Lab Chip*, 2011, **11**, 407.
6 R. Scott, P. Sethu and C. K. Harnett, *Rev. Sci. Instrum.*, 2008, **79**, 046104.
7 M. Nasir, D. A. Ateya, D. Burk, J. P. Golden and F. S. Ligler, *Biosensors and Bioelectronics*, 2010, **25**, 1363–1369.
8 J. H. Nieuwenhuis, F. Kohl, J. Bastemeijer, P. M. Sarro and M. J. Vellekoop, *Sens. Actuators, B*, 2004, **102**, 44–50.
9 M. Godin, F. F. Delgado, S. Son, W. H. Grover, A. K. Bryan, A. Tzur, P. Jorgensen, K. Payer, A. D. Grossman, M. W. Kirschner and S. R. Manalis, *Nature Methods*, 2010, **7**, 387–390.
10 M. A. Unger, H.-P. Chou, T. Thorsen, A. Scherer and S. R. Quake, *Science*, 2000, **288**, 113–116.
11 H. Chen, W. Gu, N. Cellar, R. Kennedy, S. Takayama and J.-C. Meiners, *Anal. Chem.*, 2008, **80**, 6110–6113.
12 J.-C. Galas, V. Studer and Y. Chen, *Microelectronic Engineering*, 2005, **78-79**, 112–117.
13 R. Rodriguez-Trujillo, C. A. Mills, J. Samitier and G. Gomila, *Microfluid. Nanofluid.*, 2006, **3**, 171–176.
14 S. Gawad, K. Cheung, U. Seger, A. Bertsch and P. Renaud, *Lab Chip*, 2004, **4**, 241.
15 T. Sun, N. G. Green, S. Gawad and H. Morgan, *IET Nanobiotechnol.*, 2007, **1**, 69–79.
16 J. Ferrer, C. Prats and D. López, *J. Biol. Phys.*, 2008, **34**, 19–37.